CLEO CONF 98-18
ICHEP98 855

Measurement of $\mathcal{B}(B \to \rho\ell\nu)$, $|V_{ub}|$, and the Form Factor Slope in $B \to \rho\ell\nu$ Decay

CLEO Collaboration

(July 21, 1998)

Abstract

Using a sample of 3.3×10^6 $\Upsilon(4S) \to B\overline{B}$ events collected with the CLEO II detector, we measure $\mathcal{B}(B \to \rho\ell\nu)$, $|V_{ub}|$, and the dimensionless form factor slope, ρ^2, in $B \to \rho\ell\nu$ decay. We find $\mathcal{B}(B^0 \to \rho^-\ell^+\nu) = (2.8 \pm 0.4 \pm 0.4 \pm 0.6) \times 10^{-4}$, $|V_{ub}| = (3.2 \pm 0.3^{+0.2}_{-0.3} \pm 0.6) \times 10^{-3}$, and $\rho^2 = 0.52 \pm 0.11 \pm 0.09 \pm 0.05$, where the errors are statistical, systematic, and that due to model dependence, respectively. The method used is primarily sensitive to $B \to \rho\ell\nu$ decays with leptons in the energy range between 2.3 GeV and 2.7 GeV.

C. P. Jessop,[1] K. Lingel,[1] H. Marsiske,[1] M. L. Perl,[1] V. Savinov,[1] D. Ugolini,[1] X. Zhou,[1] T. E. Coan,[2] V. Fadeyev,[2] I. Korolkov,[2] Y. Maravin,[2] I. Narsky,[2] R. Stroynowski,[2] J. Ye,[2] T. Wlodek,[2] M. Artuso,[3] E. Dambasuren,[3] S. Kopp,[3] G. C. Moneti,[3] R. Mountain,[3] S. Schuh,[3] T. Skwarnicki,[3] S. Stone,[3] A. Titov,[3] G. Viehhauser,[3] J.C. Wang,[3] J. Bartelt,[4] S. E. Csorna,[4] K. W. McLean,[4] S. Marka,[4] Z. Xu,[4] R. Godang,[5] K. Kinoshita,[5] I. C. Lai,[5] P. Pomianowski,[5] S. Schrenk,[5] G. Bonvicini,[6] D. Cinabro,[6] R. Greene,[6] L. P. Perera,[6] G. J. Zhou,[6] S. Chan,[7] G. Eigen,[7] E. Lipeles,[7] J. S. Miller,[7] M. Schmidtler,[7] A. Shapiro,[7] W. M. Sun,[7] J. Urheim,[7] A. J. Weinstein,[7] F. Würthwein,[7] D. E. Jaffe,[8] G. Masek,[8] H. P. Paar,[8] E. M. Potter,[8] S. Prell,[8] V. Sharma,[8] D. M. Asner,[9] J. Gronberg,[9] T. S. Hill,[9] D. J. Lange,[9] R. J. Morrison,[9] H. N. Nelson,[9] T. K. Nelson,[9] J. D. Richman,[9] D. Roberts,[9] B. H. Behrens,[10] W. T. Ford,[10] A. Gritsan,[10] H. Krieg,[10] J. Roy,[10] J. G. Smith,[10] J. P. Alexander,[11] R. Baker,[11] C. Bebek,[11] B. E. Berger,[11] K. Berkelman,[11] V. Boisvert,[11] D. G. Cassel,[11] D. S. Crowcroft,[11] M. Dickson,[11] S. von Dombrowski,[11] P. S. Drell,[11] K. M. Ecklund,[11] R. Ehrlich,[11] A. D. Foland,[11] P. Gaidarev,[11] R. S. Galik,[11] L. Gibbons,[11] B. Gittelman,[11] S. W. Gray,[11] D. L. Hartill,[11] B. K. Heltsley,[11] P. I. Hopman,[11] J. Kandaswamy,[11] D. L. Kreinick,[11] T. Lee,[11] Y. Liu,[11] N. B. Mistry,[11] C. R. Ng,[11] E. Nordberg,[11] M. Ogg,[11,*] J. R. Patterson,[11] D. Peterson,[11] D. Riley,[11] A. Soffer,[11] B. Valant-Spaight,[11] A. Warburton,[11] C. Ward,[11] M. Athanas,[12] P. Avery,[12] C. D. Jones,[12] M. Lohner,[12] C. Prescott,[12] A. I. Rubiera,[12] J. Yelton,[12] J. Zheng,[12] G. Brandenburg,[13] R. A. Briere,[13] A. Ershov,[13] Y. S. Gao,[13] D. Y.-J. Kim,[13] R. Wilson,[13] H. Yamamoto,[13] T. E. Browder,[14] Y. Li,[14] J. L. Rodriguez,[14] S. K. Sahu,[14] T. Bergfeld,[15] B. I. Eisenstein,[15] J. Ernst,[15] G. E. Gladding,[15] G. D. Gollin,[15] R. M. Hans,[15] E. Johnson,[15] I. Karliner,[15] M. A. Marsh,[15] M. Palmer,[15] M. Selen,[15] J. J. Thaler,[15] K. W. Edwards,[16] A. Bellerive,[17] R. Janicek,[17] P. M. Patel,[17] A. J. Sadoff,[18] R. Ammar,[19] P. Baringer,[19] A. Bean,[19] D. Besson,[19] D. Coppage,[19] C. Darling,[19] R. Davis,[19] S. Kotov,[19] I. Kravchenko,[19] N. Kwak,[19] L. Zhou,[19] S. Anderson,[20] Y. Kubota,[20] S. J. Lee,[20] R. Mahapatra,[20] J. J. O'Neill,[20] R. Poling,[20] T. Riehle,[20] A. Smith,[20] M. S. Alam,[21] S. B. Athar,[21] Z. Ling,[21] A. H. Mahmood,[21] S. Timm,[21] F. Wappler,[21] A. Anastassov,[22] J. E. Duboscq,[22] K. K. Gan,[22] T. Hart,[22] K. Honscheid,[22] H. Kagan,[22] R. Kass,[22] J. Lee,[22] H. Schwarthoff,[22] A. Wolf,[22] M. M. Zoeller,[22] S. J. Richichi,[23] H. Severini,[23] P. Skubic,[23] A. Undrus,[23] M. Bishai,[24] S. Chen,[24] J. Fast,[24] J. W. Hinson,[24] N. Menon,[24] D. H. Miller,[24] E. I. Shibata,[24] I. P. J. Shipsey,[24] S. Glenn,[25] Y. Kwon,[25,†] A.L. Lyon,[25] S. Roberts,[25] and E. H. Thorndike[25]

[1]Stanford Linear Accelerator Center, Stanford University, Stanford, California 94309
[2]Southern Methodist University, Dallas, Texas 75275
[3]Syracuse University, Syracuse, New York 13244
[4]Vanderbilt University, Nashville, Tennessee 37235
[5]Virginia Polytechnic Institute and State University, Blacksburg, Virginia 24061
[6]Wayne State University, Detroit, Michigan 48202

[*]Permanent address: University of Texas, Austin TX 78712.

[†]Permanent address: Yonsei University, Seoul 120-749, Korea.

[7]California Institute of Technology, Pasadena, California 91125
[8]University of California, San Diego, La Jolla, California 92093
[9]University of California, Santa Barbara, California 93106
[10]University of Colorado, Boulder, Colorado 80309-0390
[11]Cornell University, Ithaca, New York 14853
[12]University of Florida, Gainesville, Florida 32611
[13]Harvard University, Cambridge, Massachusetts 02138
[14]University of Hawaii at Manoa, Honolulu, Hawaii 96822
[15]University of Illinois, Urbana-Champaign, Illinois 61801
[16]Carleton University, Ottawa, Ontario, Canada K1S 5B6
and the Institute of Particle Physics, Canada
[17]McGill University, Montréal, Québec, Canada H3A 2T8
and the Institute of Particle Physics, Canada
[18]Ithaca College, Ithaca, New York 14850
[19]University of Kansas, Lawrence, Kansas 66045
[20]University of Minnesota, Minneapolis, Minnesota 55455
[21]State University of New York at Albany, Albany, New York 12222
[22]Ohio State University, Columbus, Ohio 43210
[23]University of Oklahoma, Norman, Oklahoma 73019
[24]Purdue University, West Lafayette, Indiana 47907
[25]University of Rochester, Rochester, New York 14627

I. INTRODUCTION

The study of exclusive semileptonic $b \to u\ell\nu$ decays is an active area of both experimental and theoretical study. These processes can be used to extract the magnitude of V_{ub}, one of the smallest and least well known elements of the Cabibbo-Kobayashi-Mashawa (CKM) quark-mixing matrix. To extract $|V_{ub}|$ from a measured decay rate requires significant theoretical input, because the matrix elements for such processes involve complicated, strong-interaction dynamics. Although the underlying $b \to u\ell^-\bar{\nu}$ decay is a relatively simple weak process, the transition between the heavy B meson and the light daughter hadron is extremely challenging to describe precisely. Nevertheless, substantial progress has been made using a variety of theoretical methods, including quark models [1,2], lattice QCD [3], and QCD sum rules [4].

Experimentally, the main difficulty in observing signals from $b \to u\ell^-\bar{\nu}$ processes is the very large background due to $b \to c\ell^-\bar{\nu}$. In the decay $B \to \rho\ell^-\bar{\nu}$, a significant fraction of events have lepton momenta beyond the endpoint for $b \to c\ell^-\bar{\nu}$, and requirements on lepton energy provide one of the most powerful tools for background suppression. However, the extrapolation from this portion of phase space to the full decay rate again requires the use of theoretical models, and it introduces a model dependence beyond that associated with simply extracting the value of $|V_{ub}|$ from the branching fraction. In this study, we begin to explore the decay dynamics of $B \to \rho\ell^-\bar{\nu}$ by measuring the distribution of q^2, the square of the mass of the virtual W. Eventually, studies of this type should reduce the model dependence on $|V_{ub}|$ by constraining the decay form factors.

CLEO [5] has previously observed the decays $B^0 \to \rho^-\ell^+\nu$, $B^+ \to \rho^0\ell^+\nu$, $B^+ \to \omega\ell^+\nu$, $B^0 \to \pi^-\ell^+\nu$, and $B^+ \to \pi^0\ell^+\nu$ (charge conjugate modes are implied here as well as throughout this paper) by measuring both the missing energy of an event and momentum to infer the momentum of the neutrino. This method obtained the measurements

$$\begin{aligned} \mathcal{B}(B^0 \to \rho^-\ell^+\nu) &= (2.5 \pm 0.4^{+0.5}_{-0.7} \pm 0.5) \times 10^{-4}, \\ \mathcal{B}(B^0 \to \pi^-\ell^+\nu) &= (1.8 \pm 0.4 \pm 0.3 \pm 0.2) \times 10^{-4}, \\ |V_{ub}| &= (3.3 \pm 0.2^{+0.3}_{-0.4} \pm 0.7) \times 10^{-3}, \end{aligned} \tag{1}$$

where the errors are statistical, systematic, and that due to model dependence. A large contribution to the $B \to \rho\ell\nu$ systematic error is associated with a possible nonresonant $B \to \pi\pi\ell\nu$ rate. In the analysis described below this uncertainty is reduced.

We report on a preliminary measurement of $\mathcal{B}(B \to \rho(\omega)\ell\nu)$, $|V_{ub}|$, and the form factor slope in $B \to \rho(\omega)\ell\nu$ decay, using a method sensitive primarily to leptons with energies above the $b \to c\ell\nu$ lepton energy endpoint. Having a higher signal efficiency, as well as higher backgrounds, this analysis is largely statistically independent of the previous CLEO II result.

II. DATA SAMPLE

The data used in this analysis were taken by the CLEO II [6] detector at the Cornell Electron Storage Ring (CESR). We use a luminosity of 3.1 fb^{-1} taken on the $\Upsilon(4S)$ resonance, as well as 1.7 fb^{-1} taken approximately 60 MeV below the $B\overline{B}$ production threshold. Data taken below the $\Upsilon(4S)$ provide a sample to study the $e^+e^- \to q\overline{q}$ (continuum) contribution at the $\Upsilon(4S)$.

The CLEO II detector was designed to measure both charged and neutral particles accurately over a large part of the 4π solid angle. A charged-track momentum resolution of $\Delta p/p = 0.6\%$ is achieved using three concentric cylindrical wire chambers within a 1.5 T magnetic field. A CsI electromagnetic calorimeter provides excellent resolution for the reconstruction of photons and π^0s. The typical π^0 mass resolution is $\sigma_{\pi^0} = 6$ MeV/c^2.

III. DECAY KINEMATICS

The matrix element for the semileptonic decay $P(Q\overline{q}) \to V(q'\overline{q})\ell\nu$ of a pseudoscalar meson, $P(Q\overline{q})$, to vector meson, $V(q'\overline{q})$, can be written as

$$\mathcal{M}(P \to V\ell\nu) = -i\frac{G_F}{\sqrt{2}}V_{q'Q}L^\mu H_\mu, \tag{2}$$

where L^μ is the leptonic current

$$L^\mu = \overline{u}_\ell(1-\gamma_5)v_\nu, \tag{3}$$

and H_μ is the hadronic current

$$\begin{aligned} H_\mu =< V(k,\epsilon)|(V-A)_\mu|P(p) >= -\epsilon^*_\mu(m_P+m_V)A_1(q^2) + (p+k)_\mu(\epsilon^*\cdot p)\frac{A_2(q^2)}{(m_P+m_V)} \\ +q_\mu(\epsilon^*\cdot p)\frac{2m_V}{q^2}(A_3(q^2)-A_0(q^2)) + 2i\epsilon_{\mu\nu\rho\sigma}\epsilon^{*\nu}p^\rho k^\sigma\frac{V(q^2)}{m_P+m_V} \end{aligned} \tag{4}$$

where

$$A_3(q^2) = \frac{m_P+m_V}{2m_V}A_1(q^2) - \frac{m_P-m_V}{2m_V}A_2(q^2) \tag{5}$$

with $A_0(0) = A_3(0)$. Terms proportional to q_μ vanish in the limit of massless leptons, so that the decay $B \to \rho\ell\nu$ is written in terms of three form factors (A_1, A_2, and V) for either electrons or muons. The amplitudes H_+, H_-, and H_0 for the vector meson to have helicity $+1$, -1, or 0 can be expressed in terms of these form factors

$$\begin{aligned} H_\pm(q^2) &= (m_P+m_V)A_1(q^2) \mp \frac{2m_Pp_V}{m_P+m_V}V(q^2), \\ H_0(q^2) &= \frac{1}{2m_V\sqrt{q^2}}[(m_P^2-m_V^2-q^2)(m_P+m_V)A_1(q^2) \\ &\quad - 4\frac{m_P^2p_V^2}{m_P+m_V}A_2(q^2)]. \end{aligned} \tag{6}$$

At large q^2, the $A_1(q^2)$ form factor dominates all three of the helicity amplitudes. The full differential decay rate for $P \to V\ell\nu$ ($V \to P_1P_2$) is given by [7]

$$\begin{aligned}
\frac{d\Gamma}{dq^2 d\cos\theta_\ell d\cos\theta_V d\chi} &= \frac{3}{8(4\pi)^4} G_F^2 |V_{q'Q}|^2 \frac{p_V q^2}{m_P^2} \mathcal{B}(V \to P_1P_2) \\
&\times \Big[(1-\cos\theta_\ell)^2 \sin^2\theta_V |H_+(q^2)|^2 + (1+\cos\theta_\ell)^2 \sin^2\theta_V |H_-(q^2)|^2 \\
&+ 4\sin^2\theta_\ell \cos^2\theta_V |H_0(q^2)|^2 \\
&- 4\sin\theta_\ell(1-\cos\theta_\ell)\sin\theta_V\cos\theta_V\cos\chi H_+(q^2)H_0(q^2) \\
&+ 4\sin\theta_\ell(1+\cos\theta_\ell)\sin\theta_V\cos\theta_V\cos\chi H_-(q^2)H_0(q^2) \\
&- 2\sin^2\theta_\ell\sin^2\theta_V\cos 2\chi H_+(q^2)H_-(q^2)\Big],
\end{aligned} \tag{7}$$

where $q^2 = (p_B - p_V)^2$, θ_ℓ is the decay angle of the lepton with respect to the W flight direction in the W rest frame, and θ_V is the decay angle of one of the pseudoscalar daughters with respect to the vector-meson flight direction in the vector meson's rest frame. Finally, χ is the angle between the decay plane of the W and that of the vector meson.

Form factors are alternatively expressed as functions of the variable

$$w \equiv \frac{m_P^2 + m_V^2 - q^2}{2m_P m_V}, \tag{8}$$

which is the relativistic γ factor for the daughter meson in the parent rest frame. Following Ligeti and Wise [8], we write the differential w distribution for $B \to \rho\ell\nu$ decay as

$$\begin{aligned}
\frac{d\Gamma(B \to \rho\ell\nu)}{dw} &= \frac{G_F^2|V_{ub}|^2}{48\pi^3}(m_B + m_\rho)^2 m_\rho^2 m_B \sqrt{w^2-1} \\
&\qquad \times \Big[2 + w^2 - 6wr + 3r^2\Big]\mathcal{F}_\rho^2(w),
\end{aligned} \tag{9}$$

where $r \equiv m_\rho/m_B$. This form is somewhat different from that typically used in studies of $B \to D^*\ell\nu$ decay [10]. The function $\mathcal{F}_\rho(w)$ depends on all three form factors, and near $w = 1$ is approximately equal to $A_1(w)$. It is useful to expand $\mathcal{F}_\rho(w)$ around $w = 1$ (zero-recoil)

$$\mathcal{F}_\rho(w) = \mathcal{F}_\rho(1)\Big[1 - \rho^2(w-1) + c(w-1)^2 + ...\Big]. \tag{10}$$

IV. EVENT SELECTION

For candidate leptons, we consider well-measured tracks with energies above 1.7 GeV and with $|\cos\theta| \leq 0.85$. The polar angle, θ, is measured with respect to the beam axis. Tracking and calorimeter measurements, along with specific ionization (dE/dx) information are combined to identify electron candidates with an efficiency of nearly 95% for the momentum range of interest. Muon candidates are required to traverse at least 7 interaction lengths of iron, resulting in an efficiency of 85% for muons with $E_\mu \geq 2.2$ GeV. The rate for misidentification of hadrons as electrons (muons) is approximately 0.1% (0.4%) per hadron.

For photon and π^0 reconstruction, we use CsI calorimeter clusters with $E_\gamma \geq 30$ MeV. The clusters must also be consistent with not coming from a charged track. Candidate π^0s are selected from $\gamma\gamma$ pairs that have a reconstructed mass within 2.5σ of the nominal π^0 mass. In addition, π^0 candidates must satisfy $E_{\pi^0} \geq 325$ MeV.

We consider hadronic candidates reconstructed in the $\pi^\pm\pi^0$ ($\rho^\pm$), $\pi^+\pi^-$ (ρ^0), $\pi^+\pi^-\pi^0$ (ω), $\pi^\pm$, and π^0 modes. To reduce combinatoric background, candidates are required to have a momentum greater than 300 MeV/c. Combinatoric background is further suppressed in the ω mode by making a cut on the $\omega \to \pi^+\pi^-\pi^0$ Dalitz amplitude. The $\pi^\pm\ell\nu$ and $\pi^0\ell\nu$ candidates are studied in order to better understand their contribution as background to $B \to \rho\ell\nu$. Our technique is less sensitive to $B \to \pi\ell\nu$ than to $B \to \rho\ell\nu$, as we will discuss below.

We separate leptons into three lepton-energy bins. We are most sensitive to $B \to \rho\ell\nu$ decays with leptons in the energy range from 2.3 GeV to 2.7 GeV (HILEP). We also examine leptons between 2.0 GeV and 2.3 GeV (LOLEP), as well as between 1.7 GeV and 2.0 GeV.

In HILEP, the dominant sources of background are continuum events and $b \to u\ell\nu$ processes other than $B \to \rho(\omega)\ell\nu$. We suppress $b \to u\ell\nu$ and $b \to c\ell\nu$ combinatoric backgrounds using the kinematics of $B \to \rho(\omega,\pi)\ell\nu$ decay. Using the constraints $E_B = E_{\text{beam}}$ and $p_\nu^2 = 0 = (p_B - p_\rho - p_\ell)^2$, we compute the angle between the B momentum direction and that of the reconstructed $Y \equiv \rho + \ell$ system (here and elsewhere, ρ represents ρ, ω, or π):

$$\cos\theta_{BY} \equiv \frac{m_B^2 + m_Y^2 - 2E_B E_Y}{2|\mathbf{p}_B||\mathbf{p}_Y|}. \tag{11}$$

We require that $|\cos\theta_{BY}| \cdot |\mathbf{p}_B| \leq 385$ MeV. For well-reconstructed signal events with a B momentum of less than 385 MeV, this cut is 100% efficient, but $b \to u\ell\nu$ (other than $B \to \rho(\omega)\ell\nu$), $b \to c\ell\nu$, and continuum events often produce unphysical values of $\cos\theta_{BY}$ and can be rejected. At CESR, the average B meson momentum is approximately 320 MeV, with a spread of 50 MeV.

We compare the neutrino candidate inferred from the $\rho + \ell$ candidate, known to within an azimuthal ambiguity about the B momentum direction, with that reconstructed using the missing momentum in the event. Using tracks and clusters found in the event, we define

$$\mathbf{p}_{\text{miss}} \equiv -\Sigma\mathbf{p}_i. \tag{12}$$

We require that the angle between the neutrino direction inferred from the two methods to be less than 0.6 radians.

Event-shape variables are used to suppress continuum events. B mesons are produced nearly at rest ($\beta \approx 0.065$) at the Υ(4S), and their decay products are uniformly distributed in solid angle. Continuum events tend to be more jet-like in shape. We choose $B\overline{B}$ events in the following ways:

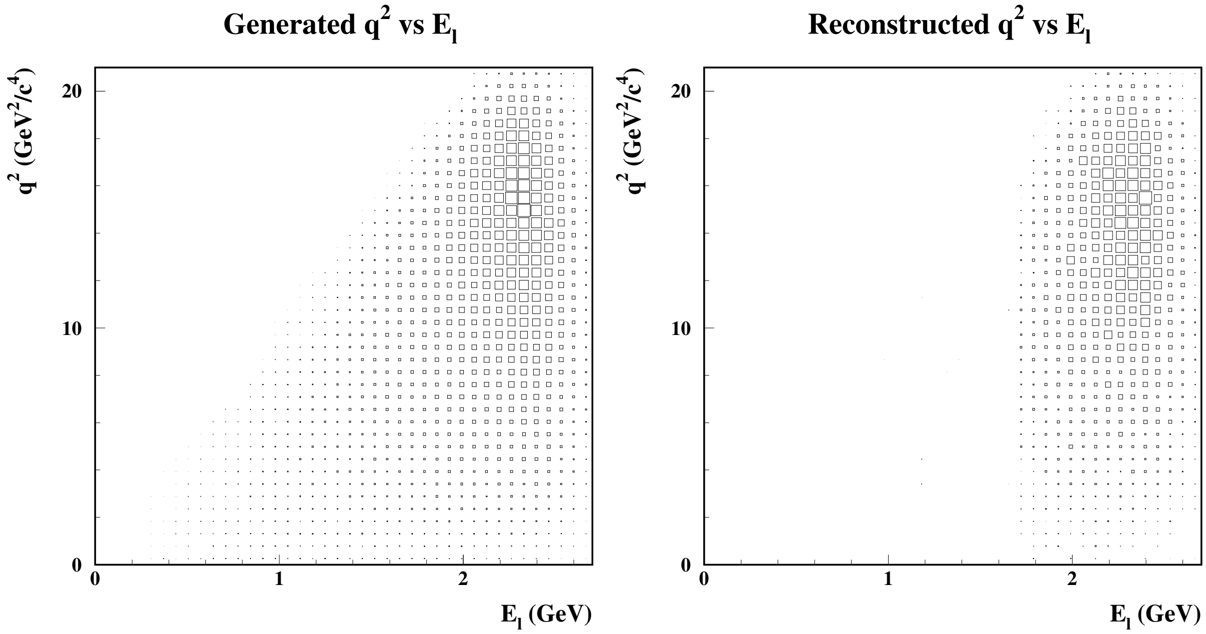

FIG. 1. Dalitz plots (q^2 versus E_ℓ) for $B \to \rho\ell\nu$ Monte Carlo (ISGW2 model). The left plot shows the generated distribution. Events that are reconstructed and pass our analysis cuts are shown in the right hand plot.

- The ratio of the second to zeroth Fox-Wolfram [11] moments is required to be less than 0.3. This ratio of moments tends to be close to zero for spherical events, and near one for jet-like events.
- $\rho\ell$, $\omega\ell$ and $\pi\ell$ candidates are required to have $|\cos\theta_{\rm thrust}| \leq 0.8$, where $\theta_{\rm thrust}$ is defined to be the angle between the thrust axis of the $\rho + \ell$ candidate and the thrust axis of the rest of the event.
- We select events with $|\cos\theta_{\rm miss}| \leq 0.9$, where $\theta_{\rm miss}$ is the polar angle of the missing momentum with respect to the beam axis (see Eq. 12).
- Events whose energy is evenly distributed around the momentum axis of the candidate lepton are chosen using a Fisher discriminant [12]. The input variables to the Fisher discriminant are both the charged and neutral particle energies in nine cones of equal solid angle around the lepton momentum axis. $B\overline{B}$ events tend to be more evenly distributed in these cones than jetty continuum events.

Figure 1 shows Monte Carlo signal events generated and reconstructed on the Dalitz plot. Figure 2 shows our signal reconstruction efficiency in HILEP as a function of w. The falloff towards large values of w is due primarily to the lepton-energy cut.

Additionally, we calculate

$$\Delta E \equiv E_\rho + E_\ell + |\mathbf{p}_{\rm miss}| - E_{\rm beam}, \tag{13}$$

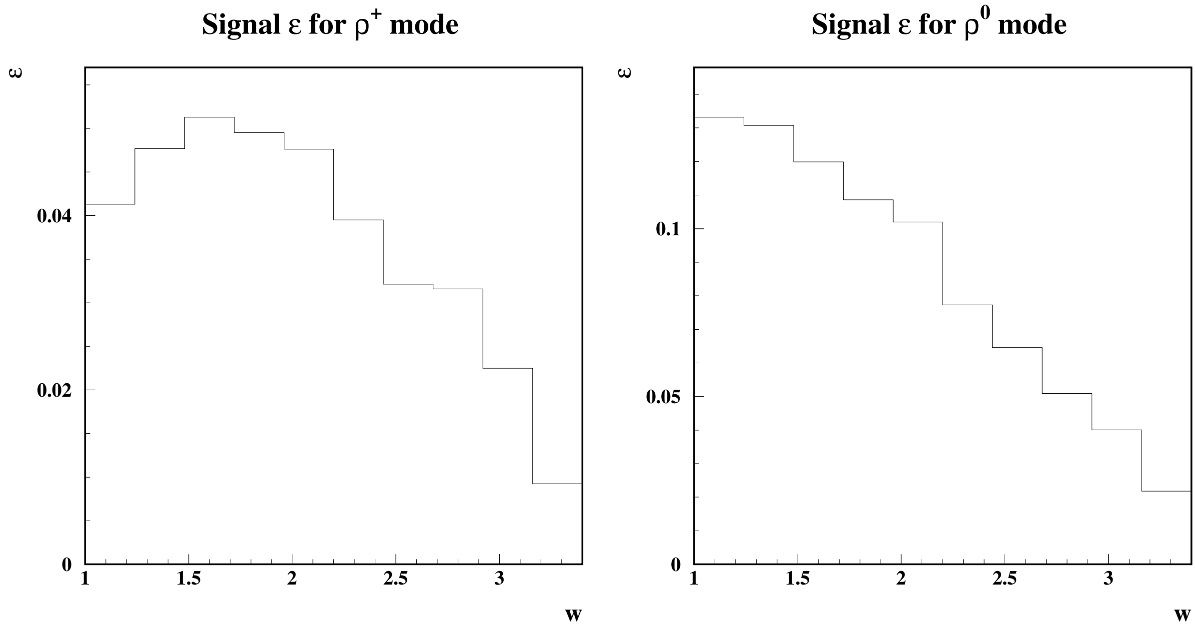

FIG. 2. The efficiency for reconstructing signal events for the $\rho^{\pm}$ (left plot) and ρ^0 (right plot) HILEP ($E_\ell > 2.3$ GeV) modes as a function of generated w is shown. The falloff towards large values of w is due primarily to the lepton-energy cut.

which is zero for true signal events within our experimental resolution. Backgrounds from $b \to c\ell\nu$ and $b \to u\ell\nu$ (other than $B \to \rho(\omega)\ell\nu$ and $B \to \pi\ell\nu$) events tend to have $\Delta E < 0$. $B \to \pi\ell\nu$ events have $\Delta E > 0$ when reconstructed in the $\pi\pi$ modes.

V. FIT TECHNIQUE

To measure $\mathcal{B}(B \to \rho\ell\nu)$ we perform a maximum-likelihood fit using MINUIT [13]. In the $\pi^{\pm}\pi^0$, $\pi^+\pi^-$, and $\pi^+\pi^-\pi^0$ modes, we fit in the variables $M(\pi\pi(\pi))$ vs. ΔE. For the $\pi^{\pm}$ and π^0 modes we perform a fit to ΔE alone. The fit is performed simultaneously in the three lepton energy ranges and five decay modes. Isospin and quark model relations are used to constrain the relative normalizations of $B^0 \to \rho^-\ell^+\nu$, $B^+ \to \rho^0\ell^+\nu$, and $B^+ \to \omega\ell^+\nu$ and separately, those of $B^0 \to \pi^-\ell^+\nu$ and $B^+ \to \pi^0\ell^+\nu$:

$$
\begin{aligned}
\Gamma(B^0 \to \rho^-\ell^+\nu) &= 2\Gamma(B^+ \to \rho^0\ell^+\nu) \\
\Gamma(B^0 \to \rho^-\ell^+\nu) &= 2\Gamma(B^+ \to \omega\ell^+\nu) \\
\Gamma(B^0 \to \pi^-\ell^+\nu) &= 2\Gamma(B^+ \to \pi^0\ell^+\nu)
\end{aligned}
\tag{14}
$$

We do not include the isospin corrections to Eq. 14 predicted in Ref. [14].

Our fit includes contributions from $B \to \rho(\omega)\ell\nu$, $B \to \pi\ell\nu$, other $b \to u\ell\nu$ modes, $b \to c\ell\nu$, the continuum, as well as a contribution from hadrons faking leptons. The continuum contribution is measured using data taken below the $\Upsilon(4S)$ resonance. The small contribution from fake leptons is also found using the data. The shapes of other contributions are modeled using a full detector simulation based on GEANT [15]. The ISGW2 [1] predictions are used to model the distributions of $b \to u\ell\nu$ sources with a hadronic mass greater than $M(\rho)$, which we will refer to as $b \to u\ell\nu$ feeddown events. We consider resonances up to the $\rho(1450)$.

We use Monte Carlo to predict the $M(\pi\pi(\pi))$ versus ΔE distributions for the $b \to c\ell\nu$ contribution in each mode. With three lepton-energy bins and five modes, there are a total of 15 $b \to c\ell^-\bar{\nu}$ normalization factors to be determined. If the Monte Carlo were known to be perfect, we would fix the normalizations to Monte Carlo predictions. Although the Monte Carlo predictions are in fact reasonably reliable, especially given that the dominant $b \to c\ell^-\bar{\nu}$ background arises from events containing the well-studied modes $\bar{B} \to D\ell^-\bar{\nu}$ and $\bar{B} \to D^*\ell^-\bar{\nu}$, we prefer to use data to fix as many parameters of the background as possible. For each of the five modes, we allow the overall scale of the $b \to c\ell^-\bar{\nu}$ background contributions to vary in the fit. In addition, we allow for a uniform (across each of the five modes) variation from the Monte Carlo prediction in the lepton energy distribution This results in two additional degrees of freedom.

There are twelve free parameters in the fit:

- $\mathcal{B}(B \to \rho\ell\nu)$ (1 parameter).
- $\mathcal{B}(B \to \pi\ell\nu)$ (1 parameter).
- The yield of $b \to u\ell\nu$ feeddown events in each lepton-energy bin (3 parameters).
- The seven parameters which describe the normalization of the $b \to c\ell\nu$ contribution as relative scale factors from the Monte Carlo prediction in each mode and lepton energy bin, as described above.

For the $B \to \rho(\omega)\ell\nu$ and $B \to \pi\ell\nu$ contributions we fix the relative number of events in each lepton-energy bin from the Monte Carlo, using a particular form factor model. The variation of the $B \to \rho\ell\nu$ form factor model is a significant systematic error for our measurement of $\mathcal{B}(B \to \rho\ell\nu)$ and $|V_{ub}|$. It is important to realize that there are a large number of crossfeed events, where events from one vector mode successfully pass the selection cuts of another vector mode. The size of the crossfeed contribution relative to the signal is found using Monte Carlo. Crossfeed events are regarded as part of the signal, although their kinematic distributions can be somewhat different from direct signal events.

$|V_{ub}|$ is calculated directly from our results for $\mathcal{B}(B \to \rho\ell\nu)$. Here again our results depend to some extent on the form factor model used for $B \to \rho\ell\nu$. We have used $\tau_{B^0} = 1.56 \pm 0.06$ ps [16].

The results of the likelihood fit are also used to extract the form factor slope. In bins of w, we consider events in the $\pi^\pm\pi^0$ and $\pi^+\pi^-$ modes with $|M(\pi\pi) - M(\rho)| \leq \Gamma(\rho)$ and $|\Delta E| \leq 500$ MeV. We then subtract the contribution of events due to continuum, $b \to c\ell\nu$,

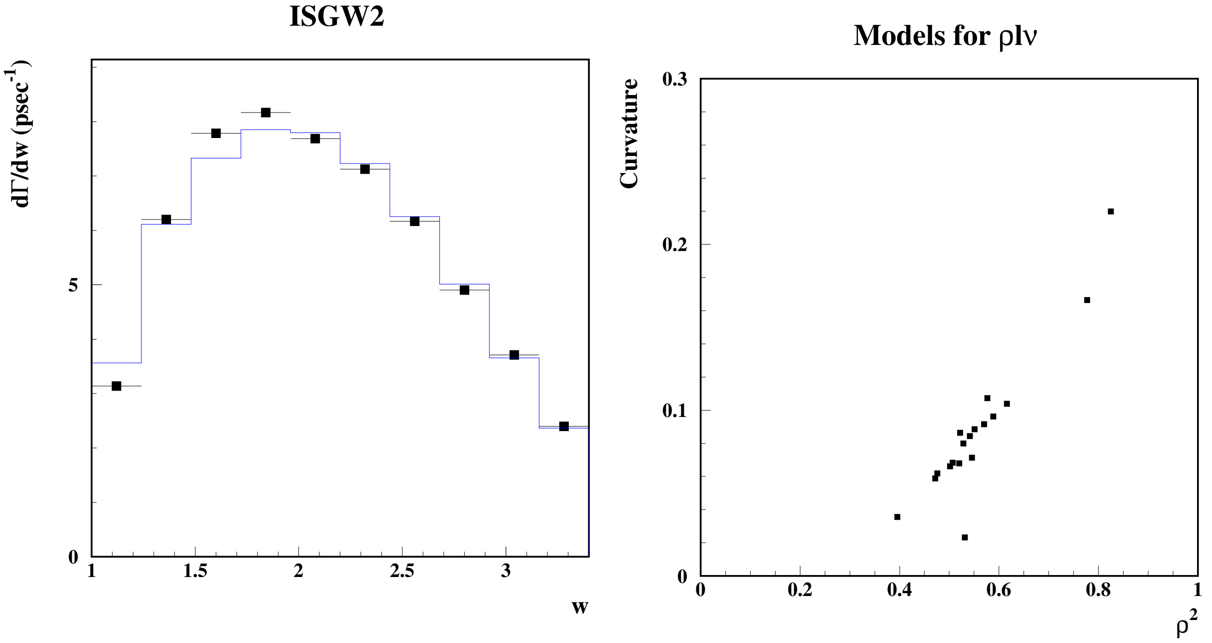

FIG. 3. The left plot shows the $d\Gamma/dw$ distribution predicted by the ISGW2 model (points) and the results (histogram) of a fit where $\mathcal{F}_\rho(w)$ is parameterized as $\mathcal{F}_\rho(1)[1-\rho^2(w-1)+c(w-1)^2]$. The right plot shows fit results for curvature and ρ^2 in Monte Carlo for the $B\to\rho\ell\nu$ form factor models that we have considered.

$b\to u\ell\nu$, $B\to\pi\ell\nu$, and fake leptons based on the results of the likelihood fit. We then compute ϵ_{ij}, our efficiency for reconstructing events in the ith w bin that were generated in the jth w bin. A form factor model must be used to correct for the efficiency of the lepton-energy cut in HILEP. We then minimize

$$\chi^2 = \sum_{i=1}^{N_{bin}} \frac{[N_i - \sum_{j=1}^{N_{bin}} \epsilon_{ij} N_j(\text{predicted}|\rho^2, c)]^2}{\sigma_i^2 + \sum_{j=1}^{N_{bin}} \sigma_{\epsilon_{ij}}^2 N_j^2(\text{predicted}|\rho^2, c)} \tag{15}$$

where $N_j(\text{predicted}|\rho^2 c)$ is the number of events predicted in the jth w bin, given ρ^2 and c.

We parameterize $\mathcal{F}_\rho(w)V_{ub}$ as

$$\mathcal{F}_\rho(w)V_{ub} = \mathcal{F}_\rho(1)V_{ub}[1-\rho^2(w-1)+c(w-1)^2]. \tag{16}$$

We do not have sufficient statistics to allow both ρ^2 and c to be free parameters in the fit. We instead use the form factor models to predict c/ρ^2, and consider variations on c/ρ^2 as a systematic error. Figure 3 shows our fit to the predicted ISGW2 w distribution as well as Monte Carlo fit results for c versus ρ^2 for the form factor models that we have considered. Table I shows the ρ^2 and c values that we obtain by fitting the predicted w distributions of various form factor models.

Model	$\Gamma/|V_{ub}|^2$ (ps^{-1})	ρ^2	c
Beyer/Melikhov [2]	16	0.56	0.09
ISGW2 [1]	14	0.53	0.07
WSB [17]	26	0.59	0.10
KS [18]	33	0.76	0.16
Ligeti/Wise+E791 [8,9]	19	0.55	0.07
Ball/Braun [20]	14	0.57	0.10
UKQCD [19]	17	0.53	0.08

TABLE I. $\Gamma/|V_{ub}|^2$, ρ^2, and c results predicted by different form factor models. The ρ^2 and c results come from our fits to the predicted q^2 distributions.

VI. RESULTS

Table II shows the results of the likelihood fit for each fit component in the $\rho^\pm$, ρ^0, and ω modes in HILEP and LOLEP. Table III shows the results for $\mathcal{B}(B \to \rho\ell\nu)$, $|V_{ub}|$, and ρ^2 for different theoretical models. Our quark model results come from an average to results in Refs. [1], [2], [17], and [18]. Lattice results, including the theoretical error, use the 1997 UKQCD form factor results in Ref. [19]. We quote results using form factors calculated using light cone sum rules (LCSR) as described in [20]. Finally, we give results using form factors due to Ligeti and Wise, using the $D \to K^*\ell\nu$ form factors measured by E791 [9], as described in [8]. The errors quoted on the quark-model results come from the variation between models. For the lattice results, we use the errors quoted in Ref. [19] on the extrapolation to low q^2. For the light cone sum rules results, our errors are taken from the shift seen between the 1997 results (in Ref. [21]) and the current results in Ref. [20]. The input w distributions for some of these models are shown in Figure 4. Our $\mathcal{B}(B \to \rho\ell\nu)$, $|V_{ub}|$, and ρ^2 results are computed from averages to the four types of form factor models that we have considered. Model dependence errors are assigned based on the range of results found with each form factor model.

Figures 5, 6, 7, 8, and 9 show projections of the likelihood fit. Good agreement is seen between the data and the fit projection both for all events in the fit and for events in the signal region. Figure 10 shows our fit to ρ^2, as well as projections of various models after efficiency and detector smearing effects have been taken into account.

As explained above, understanding $B \to \pi\ell\nu$ decay is important for the measurement of $B \to \rho\ell\nu$. Our fit result for $\mathcal{B}(B^0 \to \pi^-\ell^+\nu)$ is $(1.3 \pm 0.4) \times 10^{-4}$ (statistical error only), quite consistent with [5]. The extraction of $\mathcal{B}(B^0 \to \pi^-\ell^+\nu)$ using this method is systematics limited due to the high $b \to c\ell\nu$ backgrounds in LOLEP, and the large $B \to \rho\ell\nu$ backgrounds in HILEP (see Figure 8). Additionally, the lepton energy cut in HILEP makes any measurement of $\mathcal{B}(B^0 \to \pi^-\ell^+\nu)$ quite sensitive to the form factor model used. Given that this method would have a significantly larger systematic error than the previous CLEO study, we do not quote a full result for $\mathcal{B}(B^0 \to \pi^-\ell^+\nu)$.

	$\rho^\pm$ HI	ρ^0 HI	ω HI	$\rho^\pm$ LO	ρ^0 LO	ω LO
Υ(4S) yield	198	621	460	2249	7298	8552
Continuum bkg.	63 ± 11	248 ± 22	250 ± 22	127 ± 16	398 ± 28	437 ± 29
$b \to c\ell\nu$ bkg.	39 ± 5	90 ± 7	52 ± 5	1943 ± 27	6425 ± 49	7805 ± 49
fake lepton bkg.	4 ± 2	13 ± 7	10 ± 5	11 ± 7	35 ± 21	44 ± 22
$b \to u\ell\nu$ feeddown bkg.	24 ± 10	53 ± 23	39 ± 17	75 ± 33	170 ± 75	181 ± 80
$B \to \pi\ell\nu$ bkg.	9 ± 3	20 ± 6	4 ± 1	16 ± 5	32 ± 10	6 ± 2
Crossfeed yield	17 ± 3	82 ± 12	35 ± 5	18 ± 3	89 ± 13	53 ± 9
Fit signal yield	58 ± 9	45 ± 7	24 ± 4	58 ± 9	69 ± 10	29 ± 4
Signal Efficiency (ISGW2)	0.039	0.088	0.034	0.039	0.093	0.040

TABLE II. Summary of data yields for the $\rho^\pm$, ρ^0, and ω modes with lepton energies between 2.3 and 2.7 GeV (HILEP) and between 2.0 and 2.3 GeV (LOLEP). All yields are determined by the likelihood fit. The crossfeed contribution corresponds to events from one vector mode passing the selection cuts of another vector mode ($\rho^0\ell\nu \leftrightarrow \rho^\pm\ell\nu$ or $\rho\ell\nu \leftrightarrow \omega\ell\nu$) and is constrained to the signal in the fit. The $b \to u\ell\nu$ background includes all $B \to X_u\ell\nu$ modes except for ρ, ω, and π. All errors are statistical only. Errors on the fitted signal yield and crossfeed background are completely correlated, as are the errors on the $B \to \pi\ell\nu$ events. Errors on the $b \to u\ell\nu$ feeddown are completely correlated between modes, but not between HILEP and LOLEP. Yields for $1.7 \leq E_\ell \leq 2.0$ are not given.

VII. SYSTEMATIC ERRORS

Our systematic errors on $\mathcal{B}(B \to \rho\ell\nu)$, $|V_{ub}|$, and ρ^2 are summarized in Tables IV and V. The largest sources of systematic error come from the detector modeling in the Monte Carlo and from modeling the $b \to u\ell\nu$ contributions other than $B \to \rho\ell\nu$.

Our sensitivity to detector modeling in the Monte Carlo is due primarily to the ΔE distribution in the background contributions. We have examined the effects of changing the track and photon finding efficiencies as well as momentum resolutions. Additionally, our dependence on the response of the detector along the beampipe and the detector response to K_L's have been evaluated.

We have considered large variations in the model used for the $b \to u\ell\nu$ feeddown contribution as well as in the form factor used to describe $B \to \pi\ell\nu$. Changing the resonant makeup of the $b \to c\ell\nu$ has only a small effect. The largest sources of $b \to c\ell\nu$ are well measured modes such as $B \to D^{(*)}\ell\nu$ and $B \to J/\psi X$. Including a J/ψ veto does not change our results.

We have assigned a 5% systematic error due to our fitting method from studies where

Model used	$\mathcal{B}(B \to \rho^+ \ell\nu)$ $(/10^{-4})$	$\lvert V_{ub}\rvert$ $(/10^{-3})$	ρ^2 (DATA)
ISGW2	2.2 ± 0.4	3.2 ± 0.3	0.50 ± 0.10
Beyer/Melikhov	2.9 ± 0.5	3.1 ± 0.3	0.52 ± 0.11
WSB	3.5 ± 0.6	2.9 ± 0.2	0.52 ± 0.10
KS	2.2 ± 0.4	2.1 ± 0.2	0.65 ± 0.10
QM (Ave)	$2.7 \pm 0.4 \pm 0.4$	$2.8 \pm 0.2 \pm 0.5$	$0.54 \pm 0.11 \pm 0.04$
Lattice (UKQCD)	$2.8 \pm 0.4 \pm 0.1$	$3.3 \pm 0.3 \pm 0.3$	$0.50 \pm 0.10 \pm 0.02$
LCSR (Ball/Braun)	$3.2 \pm 0.5 \pm 0.4$	$3.8 \pm 0.3 \pm 0.1$	$0.53 \pm 0.10 \pm 0.02$
Ligeti/Wise +E791	2.5 ± 0.4	2.9 ± 0.2	0.50 ± 0.10
Average	$2.8 \pm 0.4 \pm 0.6$	$3.2 \pm 0.3 \pm 0.6$	$0.52 \pm 0.11 \pm 0.05$

TABLE III. Results for $\mathcal{B}(B \to \rho\ell\nu)$, $|V_{ub}|$, and ρ^2. The first error is statistical, and the second (where given) is due to the theoretical model uncertainty. The computation of the theoretical errors is described in the text. The model dependence errors on the averages take into account the range of results found using the different form factor models, including the theoretical error found in each catagory. The statistical errors are completely correlated, and are not reduced by averaging over form factor models. The systematic errors are not yet included (see Section VII).

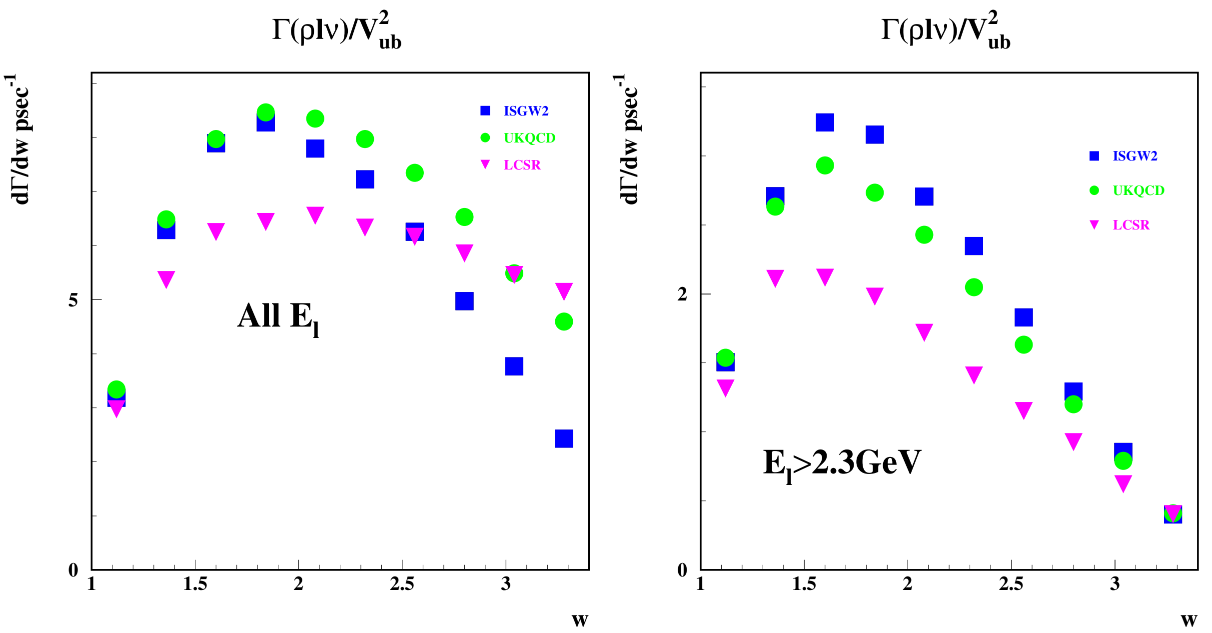

FIG. 4. The w distributions for $B \to \rho\ell\nu$ predicted by the ISGW2, UKQCD, and LCSR models. The left hand plot shows the w distribution for all leptons, and the right plot shows the w distribution for leptons in HILEP.

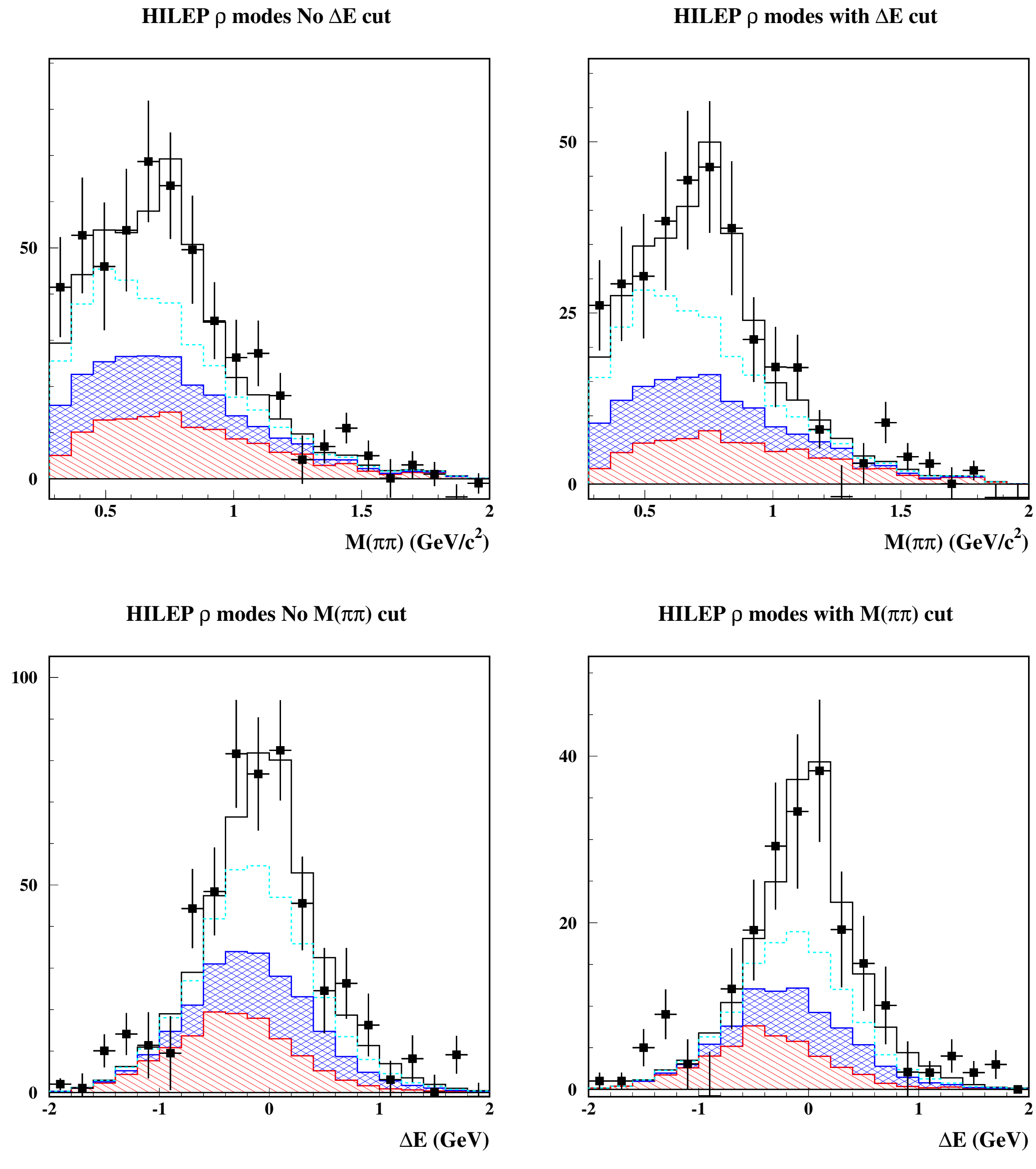

FIG. 5. Projections of the fit onto various quantities for the HILEP ($E_\ell > 2.3$ GeV) region. The upper-left histogram shows $M(\pi\pi)$ for the ρ ($\rho^\pm$ and ρ^0) modes; the upper-right histogram shows $M(\pi\pi)$ after a $|\Delta E| \le 500$ MeV cut has been applied. The lower-left histogram shows ΔE for the ρ modes; the lower-right plot shows ΔE after a $|M(\pi\pi) - M(\rho)| \le \Gamma(\rho)$ MeV cut. In each plot, the points with error bars show the on-resonance data after continuum subtraction, while the histogram shows the projection of the fit. The contributions to the fit are the direct and cross-feed components of the signal (open regions); the background from $b \to u\ell^-\bar{\nu}$ non-signal modes (double-hatched region); and the background from $b \to c\ell^-\bar{\nu}$ (single hatched region). For the $B \to \rho(\omega)\ell^-\bar{\nu}$ channels, the $b \to u\ell^-\bar{\nu}$ background includes explicit $B \to \pi\ell^-\bar{\nu}$ contributions that are tied to the signal in the $B \to \pi\ell^-\bar{\nu}$ channel.

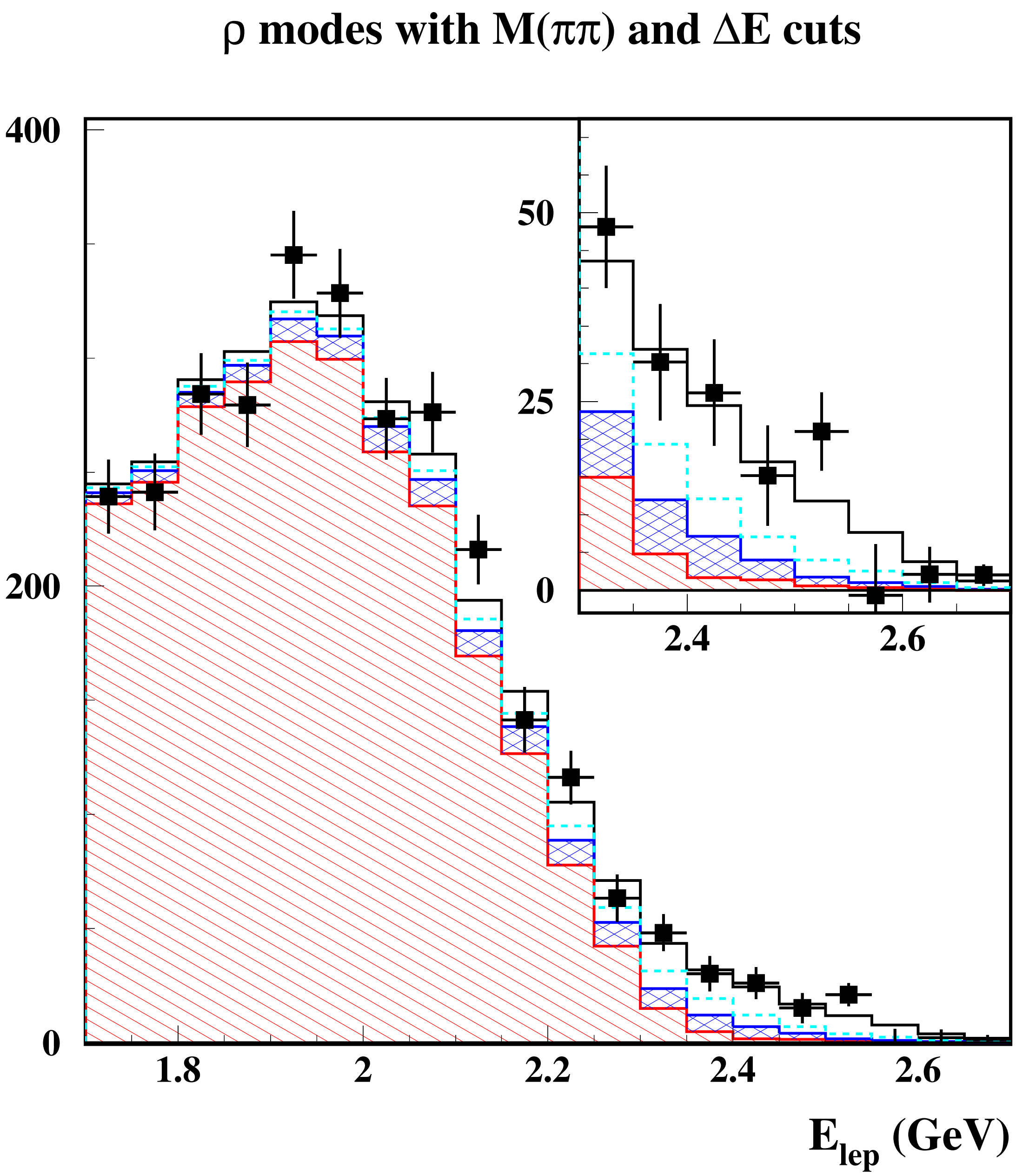

FIG. 6. Projection of the fit onto lepton energy for the $\rho^{\pm}$ and ρ^0 modes, after $|\Delta E| \leq 500$ MeV and $|M(\pi\pi) - M(\rho)| \leq \Gamma(\rho)$ cuts have been applied. The points with error bars show the on-resonance data after continuum subtraction, while the histogram shows the projection of the fit. The contributions to the fit are the direct and cross-feed components of the signal (open regions); the background from $b \to u\ell^-\bar{\nu}$ non-signal modes (double-hatched region); and the background from $b \to c\ell^-\bar{\nu}$ (single hatched region). For the $B \to \rho(\omega)\ell^-\bar{\nu}$ channels, the $b \to u\ell^-\bar{\nu}$ background includes explicit $B \to \pi\ell^-\bar{\nu}$ contributions that are tied to the $B \to \pi\ell^-\bar{\nu}$ signals.

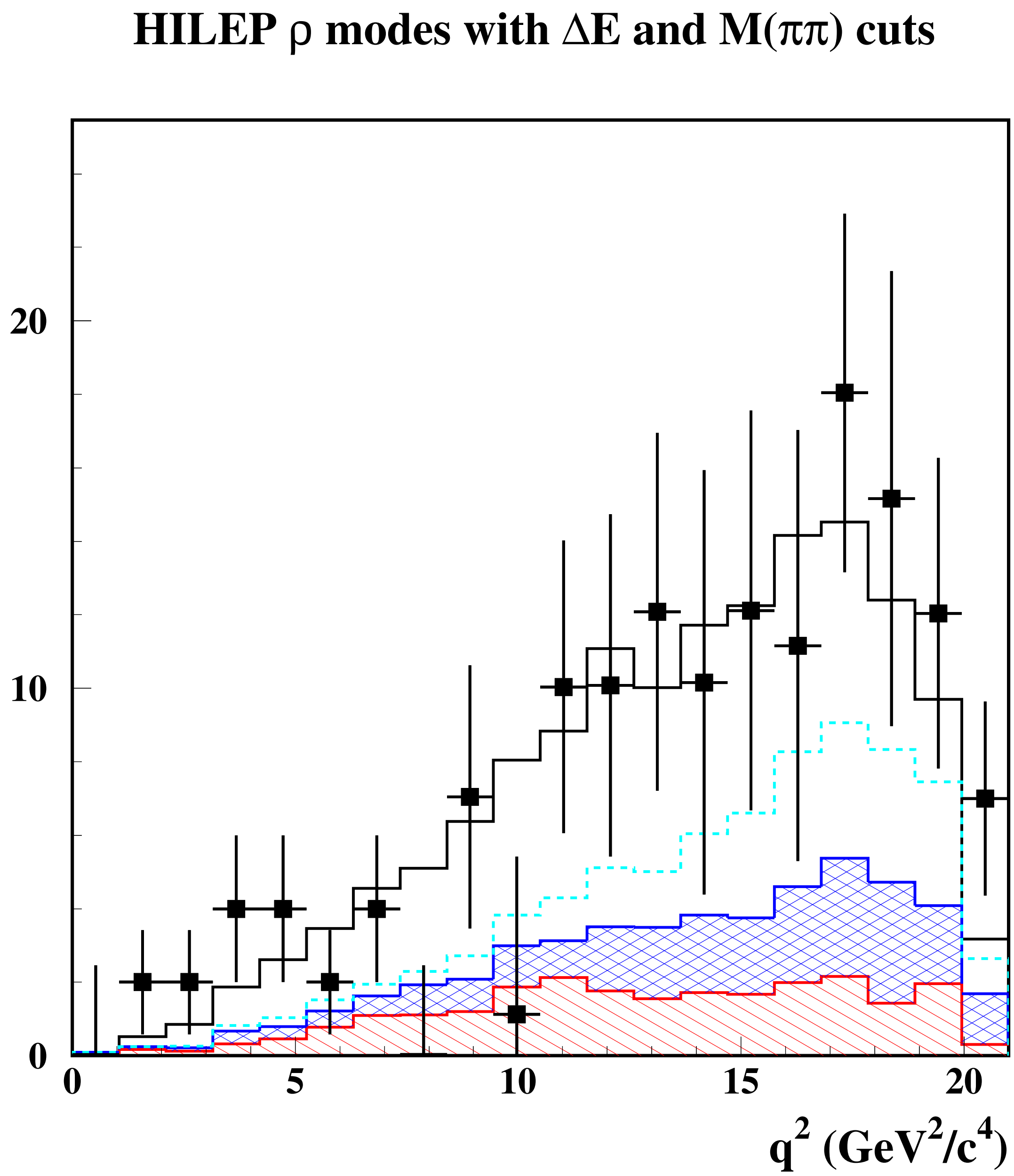

FIG. 7. Projection of the fit onto q^2 for the $\rho^{\pm}$ and ρ^0 modes, after $|\Delta E| \leq 500$ MeV and $|M(\pi\pi) - M(\rho)| \leq \Gamma(\rho)$ cuts have been applied. The points with error bars show the on-resonance data after continuum subtraction, while the histogram shows the projection of the fit. The contributions to the fit are the direct and cross-feed components of the signal (open regions); the background from $b \to u\ell^- \bar{\nu}$ non-signal modes (double-hatched region); and the background from $b \to c\ell^- \bar{\nu}$ (single hatched region). For the $B \to \rho(\omega)\ell^- \bar{\nu}$ channels, the $b \to u\ell^- \bar{\nu}$ background includes explicit $B \to \pi\ell^- \bar{\nu}$ contributions that are tied to the $B \to \pi\ell^- \bar{\nu}$ signals.

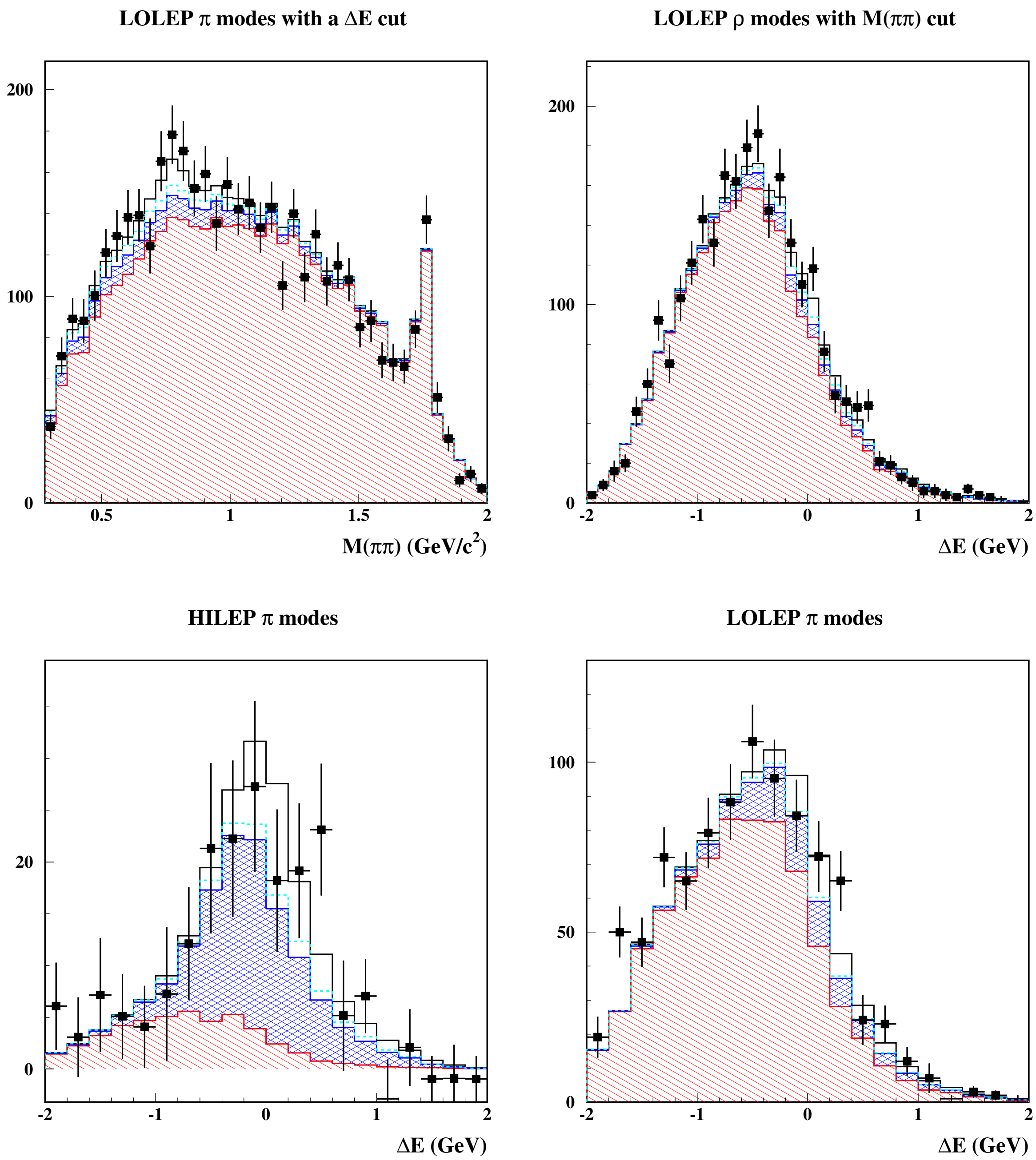

FIG. 8. Projections of the fit onto various quantities for the HILEP ($E_\ell > 2.3$ GeV) and LOLEP ($2.0 < E_\ell < 2.3$ GeV) regions. The upper-left shows $M(\pi\pi)$ for the ρ ($\rho^\pm$ and ρ^0) modes in LOLEP after a $|\Delta E| \leq 500$ MeV cut has been applied. The upper-right plot shows ΔE for the LOLEP ρ modes after a $|M(\pi\pi) - M(\rho)| \leq \Gamma(\rho)$ cut. The lower plots show ΔE in the HILEP (left) and LOLEP (right) π^+ and π^0 modes. In each plot, the points with error bars show the on-resonance data after continuum subtraction, while the histogram shows the projection of the fit. The contributions to the fit are the direct and cross-feed components of the signal (open regions); the background from $b \to u\ell^-\bar{\nu}$ non-signal modes (double-hatched region); and the background from $b \to c\ell^-\bar{\nu}$ (single hatched region). For the $B \to \rho(\omega)\ell^-\bar{\nu}$ channels, the $b \to u\ell^-\bar{\nu}$ background includes explicit $B \to \pi\ell^-\bar{\nu}$ contributions that are tied to the $B \to \pi\ell^-\bar{\nu}$ signals. For the $B \to \pi\ell^-\bar{\nu}$ channels, the background includes explicit $B \to \rho(\omega)\ell^-\bar{\nu}$ contributions that are tied to the $B \to \rho(\omega)\ell^-\bar{\nu}$ signals.

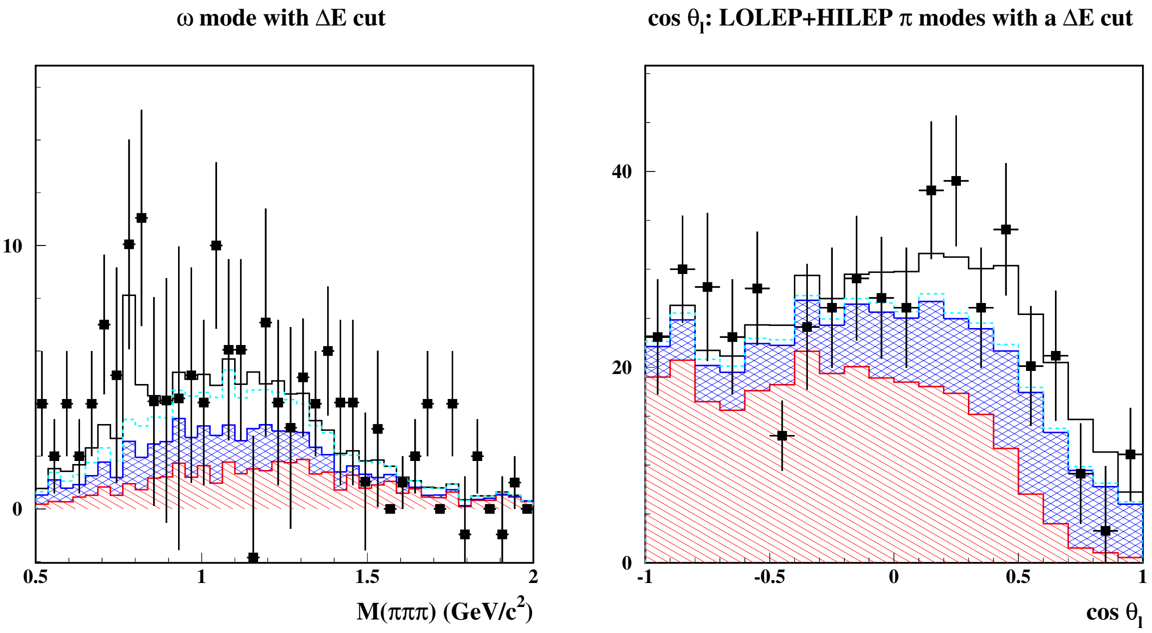

FIG. 9. Projections of the fit onto $M(\pi^+\pi^-\pi^0)$ (left plot) in the HILEP ($E_\ell > 2.3$ GeV) ω mode and $\cos\theta_\ell$ (right plot) in the HILEP+LOLEP ($E_\ell > 2.0$ GeV) $\pi^\pm$ and π^0 modes. $\cos\theta_\ell$ is the decay angle of the lepton in the W rest frame with respect to the W flight direction. In each plot, the points with error bars show the on-resonance data after continuum subtraction, while the histogram shows the projection of the fit. The contributions to the fit are the direct and cross-feed components of the signal (open regions); the background from $b \to u\ell^-\bar{\nu}$ non-signal modes (double-hatched region); and the background from $b \to c\ell^-\bar{\nu}$ (single hatched region). For the $B \to \rho(\omega)\ell^-\bar{\nu}$ channels, the $b \to u\ell^-\bar{\nu}$ background includes explicit $B \to \pi\ell^-\bar{\nu}$ contributions that are tied to the $B \to \pi\ell^-\bar{\nu}$ signals. For the $B \to \pi\ell^-\bar{\nu}$ channels, the background includes explicit $B \to \rho(\omega)\ell^-\bar{\nu}$ contributions that are tied to the $B \to \rho(\omega)\ell^-\bar{\nu}$ signals.

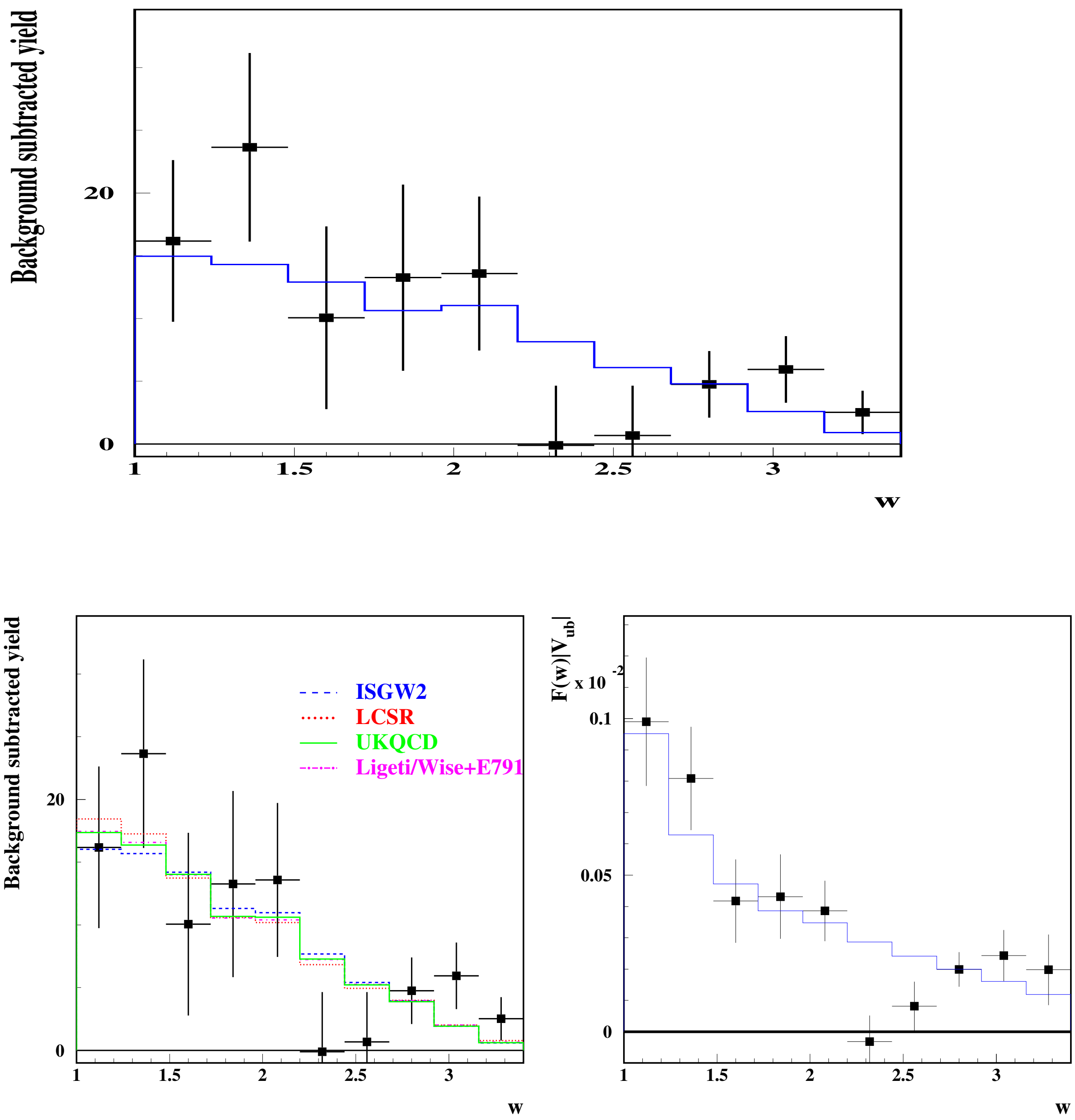

FIG. 10. The upper plot shows our HILEP background-subtracted yield is shown (points) with results of our ρ^2 fit using the ISGW2 model (histogram). The lower-left plot compares our background subtracted data (points) with predictions from various form factor models after our acceptance and smearing functions are included (histograms). The normalization of each form factor model is determined by a one parameter fit to the background subtracted data. The lower-right plot shows $\mathcal{F}_\rho(w)|V_{ub}|$ for data (points) and the fit. The data in the lower-right plot has been efficiency corrected using the ISGW2 model.

Systematic	$\delta\mathcal{B}_\rho/\mathcal{B}_\rho$ (%)	$\delta\lvert V_{ub}\rvert/\lvert V_{ub}\rvert$ (%)
Simulation of detector/$\mathbf{p}_{miss}$	$\pm 9\%$	$\pm 5\%$
$B \to c\ell\nu$ composition	$\pm 2\%$	$\pm 1\%$
$B \to X_u\ell\nu$ composition	$\pm 6\%$	$\pm 3\%$
Luminosity	$\pm 2\%$	$\pm 1\%$
Lepton Identification	$\pm 2\%$	$\pm 1\%$
Fake lepton rate	$\pm 1\%$	$\pm 1\%$
Fit technique	$\pm 5\%$	$\pm 3\%$
f_{+-}/f_{00}	$\pm 2\%$	$\pm 1\%$
$B \to \pi\pi\ell\nu$ nonresonant events	-8%	-4%
τ_B		$\pm 2\%$
Total Systematic error	$^{+13\%}_{-15\%}$	$^{+7\%}_{-8\%}$

TABLE IV. Summary of systematic errors on the $\mathcal{B}(B \to \rho\ell\nu)$ and $|V_{ub}|$ measurements.

slightly different methods were used. In particular we have explored different lepton-energy binning and the use of $\cos\theta_\ell$, the cosine of the decay angle of the lepton in the W rest frame, in the $\pi^\pm$ and π^0 modes. Our results are quite robust against changes in the fit technique.

As we use isospin and quark-model relations to determine the relative branching ratios of $B^0 \to \rho^-\ell^+\nu$, $B^+ \to \rho^0\ell^+\nu$ and $B^+ \to \omega\ell^+\nu$, our sensitivity to the ratio of charged to neutral $B\overline{B}$ events (f_{+-}/f_{00}) is quite small. We have also assigned a systematic error of 4% due to our understanding of the w distribution of our backgrounds. This error includes effects due to the generated w distribution of the $b \to c\ell\nu$ Monte Carlo.

Finally, we have assigned a conservative 8% systematic error on $\mathcal{B}(B \to \rho\ell\nu)$ due to $B \to \pi\pi\ell\nu$ nonresonant events. We determine this systematic error from several fits where a nonresonant fit component is added to the nominal likelihood fit. Several different $M(\pi\pi)$ (including a ρ Breit-Wigner) and E_ℓ distributions for the possible nonresonant component were tried. In each case, the nonresonant component determined by the fit was consistent with zero, and the increase in the statistical error on $\mathcal{B}(B \to \rho\ell\nu)$ due to the correlation with the normalization of the nonresonant component was used to determine the systematic error.

For the measurement of ρ^2 we consider the effects of changing the value of c/ρ^2 used in the fit. We have varied c/ρ^2 over a range that includes the predicted c/ρ^2 for most of the form factor models that we have considered. We assign a systematic error on ρ^2 of $\pm 14\%$. We have also assigned a systematic error of $\pm 4\%$ due to the uncertainly on the smearing of the generated w distribution. The smearing is dominanted by the B motion when the decay is reconstructed properly. In crossfeed events, however, the smearing is considerably larger.

Systematic	$\delta\rho^2/\rho^2$
Simulation of detector/$\mathbf{p}_{\rm miss}$	$\pm 5\%$
$B \to c\ell\nu$ composition	$\pm 5\%$
$B \to X_u\ell\nu$ composition	$\pm 6\%$
Fake lepton rate	$\pm 1\%$
w distribution of backgrounds	$\pm 4\%$
c/ρ^2	$\pm 14\%$
w smearing	$\pm 4\%$
Total Systematic error	$\pm 18\%$

TABLE V. Summary of systematic errors on the measurement of ρ^2.

VIII. INTERPRETATIONS AND CONCLUSIONS

We have reported on preliminary results of measurements of the exclusive $b \to u\ell\nu$ modes $B \to \rho\ell\nu$ and $B \to \omega\ell\nu$. We find

$$\begin{aligned} \mathcal{B}(B^0 \to \rho^-\ell^+\nu) &= (2.8 \pm 0.4 \pm 0.4 \pm 0.6) \times 10^{-4}, \\ |V_{ub}| &= (3.2 \pm 0.3^{+0.2}_{-0.3} \pm 0.6) \times 10^{-3}, \\ \rho^2 &= 0.52 \pm 0.11 \pm 0.09 \pm 0.05, \end{aligned} \tag{17}$$

where the errors are statistical, systematic, and due to model dependence, respectively. The branching ratio confirms the previous CLEO measurement, and is less dependent on a possible non-resonant $\pi\pi$ contribution. The measurement of the form factor slope parameter, ρ^2, represents the first form factor information extracted from the q^2 distribution in $B \to \rho\ell\nu$ decay, and agrees well with the predictions from form factor models.

The branching ratio and $|V_{ub}|$ measurements are nearly statistically independent of the previous CLEO measurement. As both analyses are sensitive only to high energy leptons ($E_\ell > 2.0$ GeV for the previous CLEO analysis, $E_\ell > 2.3$ GeV for the analysis presented here), the model dependence errors of the two analyses are highly correlated. Additionally, a large portion of the systematic errors are correlated.

We gratefully acknowledge the effort of the CESR staff in providing us with excellent luminosity and running conditions. This work was supported by the National Science Foundation, the U.S. Department of Energy, Research Corporation, the Natural Sciences and Engineering Research Council of Canada, the A.P. Sloan Foundation, the Swiss National Science Foundation, and the Alexander von Humboldt Stiftung.

REFERENCES

[1] N. Isgur and D. Scora, Phys. Rev. **D52**, 2783 (1995).

[2] M. Beyer and D. Melikhov, hep-ph/9807223, (1998); D. Melikhov, Phys. Rev. **D53**, 2160 (1996).

[3] J. M. Flynn *et al.*, Nucl. Phys. **B461**, 327 (1996).

[4] P. Ball, *et al.*, Phys. Rev. **D55**, 5561 (1997).

[5] J. P. Alexander *et al.*, Phys. Rev. Lett. **77**, 5000 (1996).

[6] Y. Kubota *et al.*, Nucl. Instrum. Methods Phys. Res. **A320**, 66 (1992).

[7] J. D. Richman and P. R. Burchat, Rev. Mod. Phys. **67**, 893 (1995).

[8] Z. Ligeti, I. W. Stewart and M. B. Wise, Phys. Lett., **B420**, 359 (1998); Z. Ligeti and M. B. Wise, Phys. Rev., **D53**, 4937 (1996).

[9] E.M. Aitala *et al.*, E791 Collaboration, Fermilab-Pub-97/267 hep-ph/9710216.

[10] In $B \to D^*\ell\nu$, $\mathcal{F}(w)$ is normalized such that in the HQET limit $\mathcal{F}(1) = 1$. $d\Gamma(P \to V\ell\nu)/dw$ is writen as
$\frac{d\Gamma(P\to V\ell\nu)}{dw} = \frac{G_F^2|V_{ub}|^2}{48\pi^3}(m_P - m_V)^2 m_V^3\sqrt{w^2-1}(w+1)^2\left[1 + \frac{4w}{w+1}\frac{m_P^2-2wm_Pm_V+m_V^2}{(m_P-m_V)^2}\right]\mathcal{F}^2(w)$.

[11] G. C. Fox and S. Wolfram, Phys. Rev. Lett. **41** 1581 (1978).

[12] R. A. Fisher, Annals of Eugenics **7**, 179 (1936).

[13] F. James, CERN Program Library Long Writeup D506, Mar. 1994.

[14] J. L. Díaz-Cruz *et al.*, Phys. Rev. **D54**, 2388 (1996), have computed isospin corrections due to ρ-ω mixing.

[15] R. Brun *et al.*, GEANT 3.15, CERN DD/EE/84-1.

[16] Particle Data Group, Phys. Rev. **D54**, 477 (1996).

[17] M. Wirbel, B. Stech, and M. Bauer, Zeit. Phys. **C29**, 627 (1985).

[18] J. G. Körner and G. A. Schuler, Zeit. Phys. **C38**, 511 (1988).

[19] L. Del. Debbio *et al.*, Phys. Lett. **B416**, 392 (1998).

[20] P. Ball, *et al.*, hep-ph/9805422, (1998).

[21] P. Ball, hep-ph/9709407 (1997). To be published in the proceedings of the 7th International Symposium on Heavy Flavor Physics.